Single nucleus pituitary transcriptomic and epigenetic landscape reveals human stem cell heterogeneity with diverse regulatory mechanisms

Zidong Zhang[1*], Michel Zamojski[2*], Gregory R. Smith[2*], Thea L. Willis[3*], Val Yianni[3*], Natalia Mendelev[2], Hanna Pincas[2], Nitish Seenarine[2], Mary Anne S. Amper[2], Mital Vasoya[2], Venugopalan D. Nair[2], Judith L. Turgeon[4], Daniel J. Bernard[5], Olga G. Troyanskaya[6,7], Cynthia L. Andoniadou[3,8], Stuart C. Sealfon[2], and Frederique Ruf-Zamojski[2]

* contributed equally

[1] Lewis-Sigler Institute for Integrative Genomics, and Graduate Program in Quantitative and Computational Biology, Princeton University, Princeton, NJ, USA

[2] Department of Neurology, Center for Advanced Research on Diagnostic Assays, Icahn School of Medicine at Mount Sinai (ISMMS), New York, NY, USA

[3] Center for Craniofacial and Regenerative Biology, King's College London, London, UK

[4] Department of Internal Medicine, University of California, Davis, CA, USA

[5] Dept. of Pharmacology and Therapeutics, McGill University, Montreal, Quebec, H3G 1Y6, Canada

[6] Department of Computer Science, Princeton University, Princeton, NJ, USA

[7] Flatiron Institute, Simons Foundation, New York, NY, USA

[8] Department of Medicine III, University Hospital Carl Gustav Carus, Technische Universität Dresden, Germany

Corresponding authors:

Frederique Ruf-Zamojski (frederique.ruf-zamojski@mssm.edu)

Stuart C. Sealfon (stuart.sealfon@mssm.edu)

Cynthia L. Andoniadou (cynthia.andoniadou@kcl.ac.uk)

Keywords:

Pituitary; stem cells; single-nucleus analysis; multiomics; transcriptome; chromatin accessibility.

Abstract

Despite their importance in tissue homeostasis and renewal, human pituitary stem cells (PSCs) are incompletely characterized. We describe a human single nucleus (sn) RNAseq and ATACseq resource from pediatric, adult, and aged pituitaries (snpituitaryatlas.princeton.edu) and characterize cell type-specific gene expression and chromatin accessibility programs for all

major pituitary cell lineages. We identify uncommitted PSCs, committing progenitor cells, and sex differences. Pseudotime trajectory analysis indicates that early life PSCs are distinct from the other age groups. Linear modeling of same-cell multiome data identifies regulatory domain accessibility sites and transcription factors (TFs) that are significantly associated with gene expression in PSCs compared to other cell types and within PSCs. Modeling the heterogeneous expression of two markers for committing cell lineages among PSCs shows significant correlation with regulatory domain accessibility for *GATA3*, but with TF expression for *POMC*. These findings characterize human stem cell lineages and reveal diverse mechanisms regulating key PSC genes.

Introduction

Tissues are composed of several cell types that can assume different gene expression states in response to environmental cues[1]. Major objectives of current biological research include resolving cellular heterogeneity within tissues and elucidating the regulatory mechanisms determining cell types and states. With the recent development of single-cell (sc) omics technologies, researchers have refined the characterization of cell types in many tissues[2, 3].

The pituitary gland secretes hormones that control crucial physiological processes, including reproduction, metabolism, and the stress response. The adenohypophysis represents the main portion of the pituitary gland and contains five hormone-producing cell lineages. Despite the physiological relevance of the pituitary in health and disease, human sc RNAseq studies to date have omitted the post-natal pituitary[4, 5]. Furthermore, mapping the pituitary epigenome

landscape has not been included in the ENCODE project[6, 7], and no chromatin accessibility profiling of the human pituitary at sc resolution has been reported.

Of particular interest is the insight into pituitary stem cells (PSCs) to be obtained from sc analyses. Pituitary hormone deficiencies, which include congenital hypopituitarism (combined pituitary hormone deficiencies), acquired hypopituitarism (secondary to trauma or surgery), as well as pituitary tumors such as adenomas, result in a severe disruption of endocrine systems and cause significant morbidity[8]. Thus, there is a need to develop stem cell therapies that could restore lost or damaged endocrine cell populations in the pituitary. Previous mouse studies demonstrated the existence of PSCs and their ability to self-renew and differentiate into all five endocrine cell types[9, 10], thus opening potential therapeutic avenues for human pituitary deficiencies and pituitary tumors[11, 12]. Little is known about the epigenetic landscape and dynamics of human PSCs during post-natal life, which is critical information for realizing their therapeutic potential. Sc studies of human pituitary are important for resolving cell identities and revealing the regulatory mechanisms of this key cell type.

One impediment to characterizing human PSC heterogeneity and elucidating gene regulatory mechanisms through sc studies is the technical difficulty in generating high-quality datasets from the frozen *post-mortem* pituitary samples provided by tissue banks. We recently developed an integrated single nucleus (sn) multi-omics analysis using frozen adult murine pituitary[13]. Here, we successfully employed a similar procedure to characterize all major cell types in the human pituitary with a particular focus on PSCs. Archived frozen *post-mortem* pituitaries from pediatric, adult, and elderly subjects (one male and one female per age group)

were jointly analyzed by snRNAseq and snATACseq (sn multi-omics). Importantly, we also generated a same-cell female pediatric pituitary sn multiome dataset. These analyses enabled us to characterize the transcriptome and chromatin accessibility landscapes of pituitary cell types. We further refined the identification of human PSC subtypes and their changes during aging and provide insight into the diverse gene regulatory mechanisms underlying stem cell identity and commitment.

Results

Sn multi-omics profiling of human pituitaries

To construct cell-type genome-wide maps of gene expression and open chromatin in the human pituitary, we conducted same-sample multi-omics assays of sn transcriptome (snRNAseq) and sn chromatin accessibility (snATACseq) in frozen *post-mortem* pituitaries from pediatric, adult, and aged individuals of both sexes that had been stored in tissue banks at -80 C for an average of ~10 years since donation (range 4 to 20; **Supplementary Table 1**). Because nuclei isolated from the same pituitary fragment were processed for both snRNAseq and snATACseq, the paired datasets, although not from the same nuclei, were sampled from the same population of nuclei in each pituitary studied. Additionally, to test for tissue heterogeneity and accuracy of cell type mapping across assays, and to improve inference of regulatory mechanisms, the remaining sample comprising nearly the entire pituitary from one female subject was pulverized and the isolated nuclei were then used to carry out: a) same-sample analysis of sn transcriptome and sn chromatin accessibility, b) same-cell sn multiome analysis providing simultaneous

114 measurement of RNA expression and chromatin accessibility within each individual nucleus
115 (**Fig. 1a**).

116 All snRNAseq and snATACseq libraries generated from the same samples were pooled
117 for sequencing to reduce batch effects. Data meeting the quality control (QC) threshold were
118 obtained from a total of 76,016 nuclei for snRNAseq and 44,141 nuclei for snATACseq in paired
119 assays, and from 15,024 nuclei in the same-cell sn multiome assay (**Supplementary Tables 2**
120 **and 3**). For data analysis of a given sample processed through the same-sample sn paired assays,
121 we generated UMAPs for both snATACseq and snRNAseq datasets, each identifying cell
122 clusters by type (**Fig. 1b, Supplementary Fig. 1**). Integration of both datasets resulted in an
123 overlay UMAP showing good correspondence of the major pituitary cell types across assay
124 modalities (**Fig. 1b, Supplementary Fig. 2**). The same-cell sn multiome assay, in which each
125 cell yielded both RNAseq and ATACseq datasets (**Fig. 1c**), directly generated an integrated
126 UMAP plot (**Fig. 1d**).

127

128 **Transcriptome analysis of human pituitary cell types**

129 The same-sample paired assay snRNAseq datasets had an average of 86% of reads
130 mapped to the transcriptome and allowed for the detection of ~2,800 genes per nucleus, with
131 comparable high-quality QC metrics obtained from all samples (**Supplementary Table 2a**). In
132 the snRNAseq data analysis of individual male and female pituitary samples, cells were clustered
133 using Seurat, visualized using t-SNE representation (**Supplementary Fig. 3**), as well as
134 projected on UMAPs (**Supplementary Fig. 1**). Cell clusters were annotated manually using
135 differential RNA expression of established pituitary marker genes. Key cell type markers

included *FSHB*, *LHB*, and *GNRHR* for gonadotropes; *GH1* for somatotropes; *POMC* for corticotropes; *DIO2* for thyrotropes[5, 14]; *PRL* for lactotropes; and *SOX9*[10], *LGR4*[15], and *RBPMS* [14] for PSCs. A list of established markers used for the assignment of each cell type as well as new markers identified in our datasets are shown in **Supplementary Table 4**. The RNA counts (**Supplementary Fig. 4**), mitochondrial gene content (**Supplementary Fig. 5**), and ribosomal protein gene content (**Supplementary Fig. 6**) all indicated the high quality of the snRNAseq data obtained from each individual donor. Cell clustering analysis revealed well-defined cell clusters, including the five major hormone-producing cell types as well as several non-endocrine cell types (**Supplementary Fig.3**).

Chromatin accessibility analysis of human pituitary cell types

The same-sample paired assay snATACseq datasets generated approximately 11,000 DNA fragments per nucleus with an average TSS enrichment score of 5.0 and a fraction of reads in called peak regions (FRiP) score of 47% (**Supplementary Table 2b**). Cells were clustered and visualized using UMAP representation (**Supplementary Figs. 1,2**). Cell clusters were manually annotated based on chromatin accessibility (i.e. peaks of accumulated reads) at informative promoters among the same marker genes used for the RNAseq annotation (see **Supplementary Table 4, Supplementary Fig. 7).** Thyrotrope cells were too poorly represented to generate reliable chromatin tracks, consistent with their being the lowest abundance endocrine cell type in the anterior pituitary[16]. Similar to the sn transcriptome analysis results, cell clustering of the snATACseq data from each donor resulted in distinct cell clusters with all the major cell types being identified, although a thyrotrope cluster could not be distinguished in all male samples (**Supplementary Figs. 1,2**).

Cell type identification in snRNAseq and snATACseq datasets

Integration of the snRNAseq and snATACseq data from each sample was accomplished by label transfer from the snRNAseq to the snATACseq data using the Seurat pipeline (**Supplementary Figs. 1,2**). The major pituitary cell type clusters were detected in all individual samples. Some clusters showed a gradient of expression and chromatin accessibility, resulting in their distinction as separate clusters, although they were not physically distinct (lactotropes in **Supplementary Fig. 3d,** corticotropes in **Supplementary Fig. 3b** and **Supplementary Fig. 1f**; somatotropes in **Supplementary Fig. 3a,c,d** and **Supplementary Fig. 1d**; pituicytes in **Supplementary Fig. 3e,f;** gonadotropes in **Supplementary Fig. 3a,d**).

To improve the resolution of human pituitary cell types and to assess inter-individual variation, we merged same-sex snRNAseq datasets and color-labeled them by donor (**Fig. 2a,c**). Similarly, we merged the snATACseq data from same-sex samples, and labeled them by donor (**Fig. 2b,d**). In addition to the five endocrine pituitary cell types, we identified stem cells, pituicytes, as well as pericytes, endothelial cells, and immune cells (macrophages, T-cells, B-cells). We observed donor-to-donor heterogeneity in cell type clustering in both datasets. For example, in males, separate gonadotrope, somatotrope, and lactotrope clusters were noted in both RNAseq and ATACseq data, originating almost exclusively from the pediatric sample. In females, one gonadotrope, one somatotrope, and one stem cell cluster were also derived from the pediatric sample. The proportions of the major pituitary cell types identified by snRNAseq vs. snATACseq across all samples were highly correlated, indicating an agreement of major cell type assignment across the two assay modalities ($R^2 > 0.96$; **Fig. 2e**). We also saw a similar

distribution of the expression markers in human pituitary cell types in comparison with the same markers in an adult mouse pituitary dataset ([13], **Supplementary Fig. 7**). A sn multiome dataset and a same-sample sn paired dataset were generated from the pulverized pediatric female sample, which further supported the reliability of cell type assignment across the two assays (**Supplementary Tables 3, 5**). All datasets are publicly available and are accessible for exploration at snpituitaryatlas.princeton.edu.

Characterization of the PSC population

The stem cells from all samples identified by snRNAseq (**Fig. 2**) were re-clustered using the Seurat pipeline, leading to the detection of 9 clusters, 6 of which were not well separated and formed a large group (**Fig. 3a**). Three clusters that are highlighted in **Fig. 3a** corresponded to lineage-committed progenitor stem cells, with each distinguished by *POMC*, *POU1F1*, and *GATA3* expression, respectively (see Discussion). The remaining large group of 6 clusters expressed *SOX2*, *SOX9,* and the Hippo pathway effectors *WWTR1* (a.k.a. *TAZ*) and *YAP1* ([17] and reviewed in [18]; **Fig. 3d** and **Supplementary Fig. 8**), which are indicative of uncommitted PSCs, with cluster 5 showing the highest expression for some of these markers.

We next examined the relationship of the PSC clusters to the sex and age of the donors (**Fig. 3b,c**). The uncommitted stem cell clusters were largely separated in samples from each sex, as confirmed by expression of the female-specific *XIST*[19]. When the male and female datasets were grouped by age, all PSC subtypes were represented at all ages studied. The distribution of RNA markers for progenitor and committing stem cells is shown in **Fig. 3d**. The canonical stem cell markers *SOX2* and *SOX9*, as well as genes previously implicated in pituitary stem cell regulation (i.e. *WWTR1*, *PITX2*, and *LGR4*; for review, see [18]), were broadly expressed.

Interestingly, expression of *JUN* and *JUND*, which were implicated in the regulation of stemness in other tissues[20, 21], was heterogeneous, with the highest expression associated with clusters that were predominant in male samples.

We also compared the patterns of marker gene expression in human and mouse PSCs. As expected, we detected *Sox2*, *Sox9*, *Wwtr1*, and *Yap1* across the stem cell population of both species (**Fig. 3d; Supplementary Figs. 8,9**). Expression of *POU1F1* in human samples was detected in a proportion of the cells in the main PSC cluster, indicating committing progenitors amongst this population, as seen for *Pou1f1* in mouse, and similarly for *PAX7*/*Pax7* (a determinant of intermediate lobe and melanotrope identity; [22]). Additional markers that were either previously reported in mouse pituitary stem cells or linked to stemness, were also found in human stem cells, including *WIF1*[23, 24], *HES1*, *NOTCH2*[18], *SMAD4*[25], and *SMAD5*[26, 27] (**Supplementary Fig. 8**).

JUN, which was expressed in uncommitted, predominantly human male PSCs, has not been proposed as a PSC marker but was previously reported to be enriched in SOX2 positive cells through bulk sequencing in mouse[15]. We therefore examined whether *Jun* showed co-expression with the stem cell marker *Sox2* by *in situ* hybridization in neonatal, juvenile male, and adult male mouse pituitaries. This analysis confirmed *Jun* as a stem cell marker by identifying *Jun*-*Sox2* double labeling in samples from all ages (**Fig. 3e** and **Supplementary Fig. 10**). Overall, characterization of the heterogeneity of the PSC population from human and mouse supports the existence of different subtypes of uncommitted stem cells that are distinguishable from early committing lineages (see [28]).

The acquisition of both snRNAseq and snATACseq data from the same samples provides high resolution analysis of the chromatin accessibility pattern of key genes within each pituitary cell type and reveals potential novel regulatory domains (see [13]). Shown in **Fig. 3f** are cell type-specific gene expression and chromatin accessibility by cell type for the stemness marker *SOX2* and the putative gonadotrope/thyrotrope committing cell lineage marker *GATA3*. *SOX2* was expressed in stem cells and pituicytes, which both showed the highest promoter accessibility. *GATA3* was expressed in gonadotropes and thyrotropes in addition to the committing stem cell lineage. All three cell types also all showed more chromatin accessibility in the region of the *GATA3* promoter. Other *SOX2* and *GATA3* putative cis-regulatory domains showing increased accessibility in cell types showing expression are also evident. In a subsequent section, we elucidate further the regulatory control of these and additional key PSC markers by modeling same-cell sn multiome data.

Diversity of PSC epigenetic programs

We next studied coordinated gene expression and chromatin accessibility programs in PSCs. We utilized the Pathway Level Information ExtractoR framework (PLIER) that deconvolves datasets into co-varying latent variable (LV) gene sets using known pathways, while not enforcing the strict orthogonality required for principal component analysis[29]. These PLIER analyses identified both RNA and chromatin accessibility LVs that were preferentially expressed in each major pituitary cell type (**Supplementary Figs. 11,12**). One RNA LV was stem cell-specific and highly expressed in both sexes at all ages (**Fig. 4a** for the top 30 genes, and **Fig. 4b** for the top 200 genes). Projection of this PSC LV onto adult mouse pituitary

snRNAseq data[13] showed conservation of this PSC transcriptome program in mouse (**Fig. 4c**). To determine whether this program was also associated with altered chromatin structure in PSCs, we projected this LV onto the human snATACseq data using the promoter accessibility signals as the gene features. This projection showed that the LV transcriptome program was associated with increased chromatin accessibility at the corresponding gene promoters (**Fig. 4d**). Analysis of the snATACseq data identified a number of largely distinct accessibility programs that were each most strongly activated in subjects of different ages or sex (**Supplementary Fig. 12**). The complexity of PSC chromatin programs identified in this analysis may be related to the diversity of the donors (see Discussion).

In addition to cell type-specific LVs, we also identified one chromatin accessibility LV showing significantly greater activity with increasing donor age ($LVage_{atac}$). Shown in **Fig. 4e** is a heat map of the 30 highest weighted promoters comprising this LV in each sample by cell type. When the level of activity in each cell type was plotted separately across the age range studied by sex, we found that all cell types showed an increase in accessibility of these promoters with age, especially between the pediatric and adult samples (**Fig. 5a**). Notably, the increases in accessibility in the PSCs were less pronounced in females, while almost no changes were observed in males (pink lines in **Fig. 5a**.) These results suggest that this accessibility program represents age-associated coordinated changes that are more prominent in differentiated cells than in PSCs.

To further explore the relationship of PSC transcriptomes in samples from different ages, we constructed a pseudotime trajectory from same-sex snRNAseq datasets using the Monocle algorithm[30] (**Fig. 5b,c**). In females as well as in males, the region of the graph most densely occupied by the pediatric PSCs was chosen as the root of the trajectory. In both sexes, pediatric

PSCs formed the largest group, which separated from the adult and aged PSCs. This separation shows the large differences between PSC transcriptomes from pediatric and adult samples and also suggests that we have not captured all transitional stages of stem cells in the samples analyzed. To specify sets of genes that are dynamically regulated as cells progress along the trajectory, we identified several correlated gene modules per age group in females and in males (**Fig. 5d**). The top genes in the most significant modules and the trajectories of selected genes are shown in **Supplementary Table 6** and **Supplementary Fig. 13**, respectively. Notably, almost none of the module-defining transcripts were previously reported as PSC markers, and their roles in PSC physiology over the lifespan are not known. Overall, these analyses show the relative stability, an aging-related chromatin program in PSCs, and dynamic changes in the PSC transcriptome with aging.

Transcription factor and epigenetic control mechanisms of PSC genes

Using snRNAseq and snATACseq datasets obtained from the same mouse pituitaries, we recently reported that chromatin accessibility is a key determinant for cell type transcriptional programs[13]. In comparison to same-sample datasets, same-cell sn multiome data confer vastly greater statistical power for inferring the regulatory mechanisms underlying expression of specific genes[31, 32]. The matched transcriptome and chromatin accessibility data in same-cell sn multiome assays allow the co-variation of chromatin accessibility and gene expression to be modeled in thousands of individual cells. Additionally, not all cells within a cell type express the same transcripts. Same-cell sn multiome data have the potential, for the first time, to provide

insight into transcription factors (TFs) and epigenetic mechanisms that shape heterogenous gene expression within the same pituitary cell type.

To explore the role of alterations in TF expression and chromatin state in modulating key PSC genes, we applied a linear modeling computational framework to the 15,024 nuclei in the same-cell sn multiome dataset obtained from a pediatric female pituitary. For each target gene, the linear model selects potential cis-regulatory regions comprising ATAC promoter peaks as well as co-accessible distal peaks. Then, testing the co-expression of putative trans-acting regulatory factors that have predicted TF binding sites in the co-accessible regions, linear regression identifies the TFs and chromatin regions most significantly predictive of expression of the target gene. The linear model, when used to analyze all pituitary cells ("pan pituitary cell" analysis), can infer the mechanisms and factors implicated in cell type-specific expression. When only cells comprising one pituitary cell type are analyzed, the linear model can generate hypotheses for the mechanisms responsible for differential expression among the different cells comprising this lineage.

We first analyzed the committed progenitor markers *POMC*, *POU1F1*, *TBX19*, and *NR5A1*. The output of the linear model pipeline is the p-value that each selected cis-regulatory region and each individual TF with sites in that region contribute to the expression of the target gene (**Supplementary Figs. 14-17**). The TFs contributing to cell type-specific expression of these marker genes using pan pituitary cell analysis included many factors that were previously implicated in the differentiation of committing stem cells. For example, the *POMC* analysis identified TBX19, which is an inducer of the *POMC*-expressing corticotrope/melanotrope lineage and of *POMC* expression[33]. *TCF7L2*, which was highly significant in the analyses of *POU1F1* and *TBX19*, is an effector of the WNT signaling pathway, which regulates pituitary

growth and development[34]. Similarly, *LEF1*, another mediator of WNT signaling (see [35]), was also identified in the *TBX19* analysis. ESR1 (estrogen receptor alpha) was the most significant TF implicated in *NR5A1* expression. Consonant with this finding, a recent study in murine gonadotrope cell lines demonstrated that estrogen-dependent binding of this nuclear receptor to a newly identified enhancer region triggers *Nr5a1* expression during gonadotrope lineage specification[36]. The high significance obtained in the linear model analysis for transcriptional regulators that were reported in previous research suggests that new candidates we identified warrant consideration for future study. For example, the TF showing the second highest significance in the pan pituitary cell analysis of *POMC* is MNX1, an important homeobox gene previously implicated in motor neuron, pancreas, and lymphoid cell development[37, 38, 39]. Therefore, MNX1 is an intriguing new candidate transcriptional regulator in the commitment towards the corticotrope/melanotrope lineages. In addition to the identification of novel putative TF regulators, when applied to all pituitary cells, the model also specifies the proximal and distal regulatory sites significantly associated with expression of the target gene in the cell types expressing that gene. These analyses identify previously unexplored regulatory domains in these key PSC genes that show accessibility associated with gene expression and are therefore cis-regulatory domain candidates (**Fig. 6** and **Supplementary Figs. 14-18**).

We next studied the stemness marker *SOX2* and the committing cell lineage marker *GATA3*. When all pituitary cells were examined, the expression of *SOX2* within the overall stem cell subtype was associated with highly significant co-accessible proximal, upstream, and downstream regulatory domains (**Fig. 6a,** *Left*) as well as expression of TFs mapping to these domains (**Fig. 6a,** *Right*). These results indicate that PSC-specific expression of *SOX2* depends on a pattern of chromatin accessibility of regulatory domains present within these cells as well as

expression of the requisite regulatory factors interacting with these domains. A contrasting result was obtained when applying the linear model to only PSCs to infer the regulatory circuits involved in heterogeneous expression of *SOX2* within PSCs. In this analysis, cis-regulatory domains correlated poorly with *SOX2* expression (**Supplementary Fig. 18,** *Left*), and a restricted set of regulatory factors (**Supplementary Fig. 18**, *Right*) was implicated in the heterogeneous pattern of *SOX2* expression in PSCs. These results suggest that the chromatin structure is sufficient for *SOX2* expression in all PSCs and the expression within specific PSCs depends on the expression of key regulatory TFs. When performing a pan pituitary cell analysis for *GATA3*, we observed a pattern consonant with that of *SOX2*, with both chromatin structure and regulatory factor expression being responsible for expression in PSCs (**Fig. 6b**, *Left*, **Fig. 6b**, *Right*). However, contrary to *SOX2*, heterogenous *GATA3* expression within PSCs was associated with cis-regulatory chromatin accessibility domains, but not with expression of specific regulatory factors (**Fig. 6c**). These results suggest that the regulatory proteins needed for *GATA3* expression in PSCs were expressed in all of the cells, and the heterogeneous expression pattern within PSCs was determined by differences in chromatin accessibility of regulatory domains between *GATA3*-expressing and non-expressing PSCs. When *POMC* was analyzed only in PSCs, the most significant TFs identified were E2F4[40] and TBX19, while the co-accessible regulatory regions were of low significance (**Fig. 6d**). These results suggest that differential *POMC* expression in committing PSCs vs. uncommitted PSCs is due to expression of these key TFs more so than to alterations in chromatin accessibility at key regulatory regions.

Discussion

We generated high quality snRNAseq and snATACseq datasets from individual human pituitaries, demonstrating the feasibility of sn profiling in frozen *post-mortem* samples that had been stored at -80 C for as long as two decades. Analysis of these data provides insight into the heterogeneity of PSCs and the regulatory mechanisms and circuits underlying the expression of key PSC genes. We distinguish and characterize uncommitting and committing stem cell lineages, differences related to the age and the sex of the donors, and propose diverse mechanisms responsible for expression of key PSC markers.

Reclustering of the stem cells identified by snRNAseq data analysis distinguishes three clusters consistent with committing stem cells (see **Fig. 3a**). The *POMC*-expressing cluster is likely a precursor of the corticotrope/melanotrope lineages[41]. Another cluster expressing *POU1F1* represents PSCs with the potential to commit to the somatotrope, lactotrope, and thyrotrope lineages[42]. The *GATA3*-expressing cluster presumably comprises cells that are committing to the gonadotrope lineage, although low expression of *NR5A1* precludes definitive cell type lineage assignment as *GATA3* is also reported in thyrotropes (**Supplementary Fig. 8**)[43]. All three committing lineages were identified in both sexes. The uncommitted stem cells, which formed six clusters that were not well separated, were for the most part non-overlapping in male vs. female samples.

Our analysis identifies PSC transcriptome and epigenetic programs as well as age-related differences in PSCs. We identify one RNAseq PSC LV program that is well expressed in all samples assayed, conserved in mouse and associated with PSC-specific chromatin changes at the promoters for the genes comprising this LV. We also identify an ATACseq LV that exhibits increased accessibility with age in all pituitary cell types but shows smaller changes with age in PSCs. When the snRNAseq data were analyzed by trajectory, PSCs from the pediatric samples

were separated from the adult and aged samples in both sexes. We find that human and mouse PSCs shared similar patterns of gene expression and were characterized by the presence of several subtypes of uncommitted and committed cells, suggesting a high degree of conservation of this cell type in evolutionary time. However, the identification of species-specific genes might signify inter-species or age-related differences, with potential implications for using the mouse model for therapy development.

The PSC LV programs, and the complete separation of PSCs across different ages in the trajectory analysis, indicate that fully characterizing the changes in PSC transcriptional and epigenetic programs with aging will require analysis of additional samples over the age span. Collectively, our data suggest that sex and age influence several biological processes in stem cells. Additional study is warranted to further elucidate the sex and age differences that are likely to have a significant impact on the development of new stem cell-based therapies.

The datasets generated encompass all major cell types in the human pituitary. Reliability of the identification of all major cell types in the same-sample snRNAseq and snATACseq datasets from both sexes and from a range of subject ages is supported by the concordance of cell type proportions obtained by both assays and the confirmation of cell type identification in the same-cell sn multiome data. We report gene expression and chromatin accessibility LVs that are characteristic of each major pituitary cell type. Extensive data from the female pediatric pituitary are provided by multiple same-sample datasets and a large same-cell sn multiome dataset. These data represent a resource to address questions about the characterization and regulatory mechanisms of any cell type in the human pituitary.

Inferences from the same-cell sn multiome dataset using the linear model provides insight into the TFs and accessible chromatin sites contributing to the expression of key PSC genes. The model also provides insight into the general mechanisms (TF expression, chromatin accessibility differences or both) responsible for differential expression of the target PSC genes among different cells. Because the model is based on detection of regulatory feature correlation with target gene expression, the results obtained when PSC genes are analyzed among all pituitary cells represent mechanisms implicated in target gene expression in PSCs in comparison with other cell types. When the model is applied only to PSCs, the results represent hypotheses for differential expression of these target genes within a subset of PSCs. For the PSC and committed progenitor markers analyzed (*POMC, POU1F1, TBX19, NR5A1, SOX2,* and *GATA3*), multiple chromatin accessibility sites and TFs predicted to bind to accessible sites are identified with high probability as contributing to stem cell expression of these markers in comparison with other cell types. This supports the formulation that the expression of each of these markers in PSCs depends on epigenetic remodeling of chromatin as well as on expression of key TFs that are necessary for driving gene expression.

Analysis of same-cell sn multiome data from the pediatric female pituitary suggests that a diversity of mechanisms contribute to differential expression of marker genes among PSCs. With respect to differential expression of PSC markers within PSCs, *NR5A1* and *POU1F1* show TFs and chromatin sites associated with heterogeneous expression. *POMC, TBX19,* and *SOX2* are associated with the expression of specific TFs and *GATA3* with accessibility of specific regulatory sites. The pan-pituitary analysis shows the importance of both TF expression and chromatin structure in the expression of key PSC genes. However, these analyses of heterogenous expression within PSCs suggest that the differential expression of some markers is

426 predominantly determined by expression of key TFs in those cells, whereas the differential
427 expression of other markers depends on heterogeneity in chromatin structure.

428 A strength of this study is the multi-omic profiling of the entire pituitary at postnatal
429 stages, that we use to develop a map of the variation of PSCs between the sexes and with
430 development and aging. Additionally, to our knowledge, this is the first study to profile human
431 PSCs through ageing and to propose mechanisms for differential marker gene expression within
432 the same cell type. We demonstrate the power of same-sample and same-cell multiomics
433 analyses to further elucidate the mechanisms underlying PSC cell type and cell state in both
434 sexes and throughout the age span.

435

436 **Methods**

437

438 **Sample procurement**

439 Flash-frozen *post-mortem* human pituitaries were obtained from the National Institutes of
440 Health (NIH) NeuroBioBank, and kept at -80C until processing. See **Supplementary Table 1**
441 for information on subject sex, age, ethnicity, *post-mortem* interval (PMI), cause of death, and
442 year of collection. The tissues received varied from whole to pieces of pituitaries. All specimens
443 were obtained from deceased individuals. Donor anonymity was preserved, and guidelines were
444 followed regarding consent, protection of human subjects, and donor confidentiality.

445

446 **Nuclei isolation from pituitaries**

447 Two methods were tested for nuclei isolation. Frozen *post-mortem* human pituitaries
448 were either: 1) broken into small pieces in a frozen mortar on dry-ice, and one piece was thawed

449 on ice and prepared for nuclei extraction based on a modified protocol from[44], or 2) pulverized
450 and part of the powder used for nuclei isolation. The remainder of the pituitary was stored back
451 at -80C. Briefly, and all on ice, RNAse inhibitor (NEB cat# MO314L) was added to the
452 homogenization buffer (0.32 M sucrose, 1 mM EDTA, 10 mM Tris-HCl, pH 7.4, 5mM $CaCl_2$,
453 3mM $Mg(Ac)_2$, 0.1% IGEPAL CA-630), 50% OptiPrep (Stock is 60% Media from Sigma; cat#
454 D1556), 35% OptiPrep and 30% OptiPrep right before isolation. Each pituitary was
455 homogenized in a Dounce glass homogenizer (1ml, VWR cat# 71000-514), and the homogenate
456 filtered through a 40 mm cell strainer. An equal volume of 50% OptiPrep was added, and the
457 gradient centrifuged (SW41 rotor at 17,792xg; 4C; 25min). Nuclei were collected from the
458 interphase, washed, resuspended either in 1X nuclei dilution buffer for snATACseq (10X
459 Genomics) or in 1X PBS/0.04% BSA for snRNAseq, and counted (Cellometer).
460
461 **SnRNAseq assay**
462 SnRNAseq was performed following the Single Cell 3' Reagents Kits V3 User
463 Guidelines (10x Genomics, Pleasanton, CA). Nuclei were filtered and counted on a Countess
464 instrument. A minimum of 1,000 nuclei were targeted (Chromium Single Cell 3' Chip kit A v2
465 PN-12036 or v3 chip kit B PN-2000060). Reverse-transcription (RT) was performed in the
466 emulsion, cDNA amplified, and libraries constructed with v3 chemistry. Libraries were indexed
467 for multiplexing (Chromium i7 Multiplex kit PN-12062).
468
469 **SnRNAseq data analysis**
470 SnRNAseq data were processed using the Cell Ranger pipeline v5.0.0, and aligned to the
471 Cell Ranger GRCh38 reference genome, introns included. Clustering and differential gene

expression analysis were performed using Seurat v.3.9.9.9024 and standard procedures[45, 46]. Top markers for each cluster were compared to known markers of pituitary cell types to annotate the clusters; a list of the most common genes associated to each cell type is given in **Supplementary Table 4**.

We used the t-SNE projection to identify the most common cross-type doublets, as well as apoptotic and low-count cells as t-SNE preserves the local structure of the data better than the UMAP projection. Doublet clusters appear as small, high UMI count satellites to the main clusters. We verified the nature of every such group of cell barcodes by plotting their gene expression of the top cell-type markers. By looking at which two gene expression programs are expressed in the barcodes composing each one of these satellite clusters, we were able to identify the two cell types that constitute the barcodes of these sub-clusters.

Apoptotic cells form their own clusters separate from the parent cluster. Several cell types often merge into a single apoptotic cluster, so that not every cell type will have its corresponding apoptotic cluster. These cells are characterized by low UMI counts and almost exclusively spliced mRNA reads, suggesting condensation of the nuclei and arrest of transcription of new mRNA.

Some cell-type clusters have offshoots composed of barcodes with low UMI counts. Contrary to apoptotic clusters, these have a similar ratio of intronic to exonic reads as their parent cluster and do not form their own cluster, but usually connect to, or appear very close to, their parent cluster. These are probably experimental artifacts of slow mRNA capture. Their gene expression program is the same as that of their higher UMI counterparts, but they are more adversely affected by dropouts. As such, we decided to remove these low-UMI offshoots from downstream analysis, together with doublet barcodes and apoptotic cells.

SnATACseq assay

SnATACseq was performed following the Chromium Single Cell ATAC Reagent Kits V1 User Guide (10x Genomics, Pleasanton, CA). Nuclei were counted (Countess counter), transposition was performed in 10 µl at 37C for 60min on at least 1,000 targeted nuclei, before loading of the Chromium Chip E (PN-2000121). Barcoding was performed in the emulsion (12 cycles) following the Chromium protocol. Libraries were indexed for multiplexing (Chromium i7 Sample Index N, Set A kit PN-3000262).

SnATACseq analysis

SnATACseq data were processed using Cell Ranger-ATAC pipeline version 1.2.0, and aligned to the Cell Ranger-ATAC GRCh38 reference genome. Clustering was performed using Seurat/Signac versions 3.1.5/0.2.4 and standard procedures[47]. We produced chromatin accessibility tracks around known pituitary cell type marker genes and looked for promoter accessibility of these genes to annotate the clusters.

Doublets, low-count, and apoptotic cells were identified in the same manner as for snRNAseq data, except that for ATAC data, the UMAP projection works better and was used instead. We used the number of fragments in peaks as an indicator as to whether a cell was healthy or a doublet or low-count / apoptotic. Doublets were checked to possess fragments in peaks associated to the main markers of both cell types. In general, we have many fewer cell barcodes in the ATAC data, so doublets are also less common. Consequentially, few doublet clusters were identified.

518 **Sn multiome assay**

519 Sn multiome was performed following the Chromium Single Cell Multiome ATAC and
520 Gene Expression Reagent Kits V1 User Guide (10x Genomics, Pleasanton, CA) on part of the
521 pulverized pediatric female sample. Nuclei were counted (Countess counter), transposition was
522 performed in 10 µl at 37C for 60min targeting 10,000 nuclei, before loading of the Chromium
523 Chip J (PN-2000264) for GEM generation and barcoding. Following post-GEM cleanup,
524 libraries were pre-amplified by PCR, after which the sample was split into three parts: one part
525 for generating the snRNAseq library, one part for the snATACseq library, and the rest was kept
526 at -20C. SnATAC and snRNA libraries were indexed for multiplexing (Chromium i7 Sample
527 Index N, Set A kit PN-3000262, and Chromium i7 Sample Index TT, Set A kit PN-3000431
528 respectively).

529

530 **Sn multiome analysis**

531 We analyzed the pediatric female sample by sn multiome. We pooled together libraries
532 from both GEM wells and ran the Cell Ranger ARC 1.0.0 pipeline on the pooled
533 sample following 10x Genomics guidelines. Running the pipeline on each GEM well separately
534 reveals that the samples have 97 barcodes in common that are called as cells.

535 We used Seurat version 3.9.9.9024 with Signac version 1.1.0 to perform our clustering
536 analysis using a weighted shared nearest neighbor graph approach. This method identifies, for
537 each cell, its nearest neighbors based on a weighted combination of the two modalities (Gene
538 Expression & Chromatin Accessibility). We similarly use the weighted nearest neighbor graph to
539 obtain a UMAP projection of the data. The Gene Expression modality was used to identify
540 cluster cell types after determination of top markers for each cluster.

Apoptotic, low-count cells and doublets were also identified in a manner analogous to that of snRNAseq data. Both apoptotic and low-count cells were identified as having much lower counts of both their number of transcripts as well as their number of fragments overlapping ATAC peaks. Apoptotic cells further have a large proportion of mitochondrial gene transcripts, whereas low-count cell transcripts are dominated by background genes. Doublets, on the other hand, were identified as having higher counts in both RNA and ATAC, and expressing gene programs of two cell types simultaneously. Only one of the main clusters was identified as doublets, and no further sub-clustering was attempted.

Merged datasets analysis

All male and female samples were merged by sex in Seurat at the UMI count level, and all of the clustering analysis was repeated on the merged samples independently from the beginning. We followed the same analysis steps as for individual samples. Unlike our integrated samples (see later section), the merged samples do not have batch effects removed. Despite that, we do not observe any systematic batch effect between our samples. We do, however, see differences in gene expression from one subject to another among some specific cell types. The merged samples allow us to highlight these differences in the implicated cell types.

Quality control (QC) and sequencing of libraries

Libraries were quantified by Qubit 3 fluorometer (Invitrogen) and quality was assessed by Bioanalyzer (Agilent). Equivalent molar concentrations of libraries were pooled and the reads were adjusted after sequencing the pools in a Miseq (Illumina). The libraries were then

563 sequenced in a Novaseq 6000 (Illumina) at the New York Genome Center (NYGC) following
564 10X Genomics recommendations.
565
566 **Mouse snRNAseq stem cell data analysis**
567 SnRNAseq data for each mouse were processed and analyzed as previously described[13].
568 Raw reads from each mouse sample were isolated from the clusters assigned in Seurat as 'Stem
569 cells' using the 'WhichCells' function. These count tables were integrated using Seurat (v3.1.5)
570 SCTransform workflow[48], clustered at 0.5 resolution and principal component dimensions 1:15
571 were taken forward for analysis.
572
573 **Human stem cell re-clustering method**
574 Following initial clustering of the complete datasets, the 'stem cell' clusters were isolated
575 from each individual subject using the Seurat 'subset' function. To increase the number of cells
576 available for downstream analysis, the isolated stem cell datasets were merged based on the
577 approximate age of subjects. This was performed using the merge function within Seurat
578 (v3.1.5). Sample integration by identification of anchors and subsequent clustering (20 PCAs,
579 resolution 0.5) was performed using Seurat according to standard procedures[45, 46]. Re-clustering
580 and analysis leading to identification of 'committing' stem cells was done as above following
581 removal of the 'Pars Tuberalis' cell clusters.
582
583 **RNAscope mRNA *in situ* hybridization**
584 Wildtype CD-1 murine postnatal pituitaries were dissected at P3, P15 (male), and P56
585 (male), and fixed in 10% neutral buffered formalin (Sigma) at room temperature for 16-24 hours.

Samples were washed in PBS and dehydrated through graded ethanol series before paraffin-embedding as previously described[15]. Samples were sectioned at 5 µm.

The RNAscope 2.5 HD Duplex assay (Advanced Cell Diagnostics) was used according to manufacturer's recommendations, with the following specific probes: Mm-Jun (Cat# 453561) and Mm-Sox2-C2 (Cat# 401041-C2) (Advanced Cell Diagnostics). Sections were counterstained with Mayer's hematoxylin (Vector H-3404) and mounted with Vectamount Permanent Mounting Medium (Vector H-5000).

Pseudotime sn trajectory analysis

Raw gene counts were extracted from each sample's "Stem Cell" cluster as previously identified using Seurat (v4.0.1)[49]. Due to sex differences, male and female samples were handled separately. Samples of the same sex (e.g female pediatric, female adult, female aged), were integrated using the functions '*SCTransform'* and '*SelectIntegrationFeatures'* in Seurat to obtain the top 500 differentially expressed genes (DEGs). Monocle3 (v0.2.3.0)[50] was used for pseudotime trajectory analysis and preliminary analysis revealed a bias in the Monocle trajectory due to specific hormonal genes namely; *GH1*, *PRL*, *CHGB*, *POMC*, *LHB*, *FSHB* and *CGA*. Therefore, these genes were regressed out of the top 500 DEGs. Monocle objects were generated by combining the 3 samples of each sex using the respective top 500 DEGs. The trajectory was calculated by merging partitions with the root chosen based on the earliest timepoint available for each sex. To find gene modules changing over pseudotime, the '*graph_test'* function was carried out using the neighbor_graph = "principal_graph" parameter with a resolution of 0.8 for '*find_gene_modules'* function. The top 4 enriched modules for each age in each sex were

608 highlighted and examined further because they showed the highest variability between age
609 groups.
610
611 **PLIER data analysis**
612 To examine more deeply the trends in gene expression of assigned cell types across
613 samples and data types, we treated each sc dataset as a collection of bulk datasets for given
614 labeled cell types. Each cell type was then treated as a separate bulk measurement within each
615 sample. For snATACseq data, peak counts for a given gene were generated by selecting the peak
616 closest to the transcription start site (TSS). These peak counts per gene were then collected into
617 single bulk measurements for each cell type in each sample. We focused specifically on six
618 relevant cell types in the pituitary: corticotropes, gonadotropes, lactotropes, somatotropes,
619 stem/progenitor cells, and thyrotropes. For the snRNAseq dataset, this process generated 36 bulk
620 measurements over six samples (three females and three males), and for the snATACseq dataset,
621 we generated 35 bulk measurements as thyrotropes were not identified in the male adult
622 snATACseq sample. We applied PLIER[29], which finds patterns in count data that are associated
623 with known prior information (such as Reactome and Kegg), focusing on the 2000 genes with
624 the highest standard deviation in count values across the bulk measurements in each set of
625 samples. PLIER was run on each set of samples separately with LVs generated on the bulk
626 measurements in an unsupervised fashion. LVs were then curated to find patterns relevant to
627 individual cell types as well as sample-wide trends such as sex-based differences. Statistical
628 significance of LVs was computed through the Kruskal-Wallis non-parametric test for multiple
629 groups as part of the stat_compare_means R method. Comparisons between LVs within and

630 across datatypes were achieved by comparing the overlap of the 200 genes most associated with
631 a given LV.

632 B is a PLIER-derived expression value for the genes associated with a given LV across
633 the different samples. It can be treated similar to average expression, weighted by gene
634 association with the LV. Technically, B is a matrix of size #LVs x #Samples. It is one of two
635 matrices in PLIER, along with Z of size # of genes x #LVs. The goal of PLIER is to find values
636 of B and Z that minimize the equation ||Y - Z*B|| where Y is our data matrix of size #genes x
637 #samples. So PLIER finds a suitable number of LVs that can be used to connect the genes and
638 samples and accurately estimate our data matrix.

639 For the boxplot statistical analysis (**Supplementary Fig.12**), ggboxplot generates a
640 boxplot with the center equal to the 50th percentile, the bounds of the box are the 25th and 75th
641 percentile and the bounds of the whiskers are the smallest/largest values 1.5 times the
642 interquartile range below the 25th percentile or above the 75th percentile, respectively.

643

644 **Sn data integration**

645 The snRNAseq and snATACseq data were integrated in a reference-query based manner,
646 mainly using the "FindTransferAnchors" and "TransferData" functions from the Seurat v3
647 package[45, 46]. The snRNAseq datasets were used as the reference and the other modalities were
648 integrated to them. To integrate snATACseq to snRNAseq, the peak-by-cell accessibility matrix
649 was converted to a gene-by-cell activity matrix based on the chromatin accessibility within each
650 gene's gene body and a 2kb upstream region, under the assumption that chromatin accessibility
651 and gene expression were positively correlated. The variable features from the snRNAseq data

were used to find the anchors and the snATACseq data in the LSI low-dimensional embedding were used to transfer the data from snRNAseq to snATACseq.

Linear modeling analysis

The regulatory model of gene expression from the sn multiome dataset was constructed for each target gene with multiple steps: 1) A list of potential regulatory genomic regions were selected. They included: a) any ATAC peaks that overlaped with the TSS +/- 2kb region, b) distal peaks that were no more than 500kb away from the TSS and were co-accessible with any of the peaks in a). Co-accessibility scores were calculated using the Cicero package [51] with default parameters, and a cutoff of 0.25 for the co-accessibility scores were used to select co-accessible peaks. 2) A list of potential regulatory TFs was selected by scanning for TF binding sites in the selected genomic regions using the "matchMotifs" function (with a p value cutoff of 5e-5) from the r package "motifmatchr" and the position weight matrices (PWMs) from the JASPAR CORE database. 3) Linear regression was used to model the target gene's expression across cells as a function of selected TFs' expression and ATAC peaks' openness, and the coefficients from the regression were used to measure the importance of each TF and genomic region. SCTranform[48] normalized RNA counts and TFIDF normalized ATAC peak counts were used in the regression.

Statistics

In **Fig. 5a**, to calculate the statistical significance of expression or accessibility changes within a given latent variable, we applied two-way ANOVA for multiple group testing and Tukey test for pairwise comparisons. Each test was applied to female and male samples

675 separately. In both cases, we applied the R statistical functions *aov* and *TukeyHSD* with the
676 additive model *Expression ~ 'Cell Type' + 'Age Group'* for the calculations.

677 In **Supplementary Figs. 11a** and **12a**, the hierarchical clustering of the LV B scores was
678 accomplished through the default complete linkage method utilized by the R function *pheatmap*.

679 For the boxplots analysis in **Supplementary Fig. 12c**, the analysis was done with n=3
680 independent subjects per sex and statistical analysis using the Wilcoxon ranked-sum test.

681 **For Fig. 6 and Supplementary Figs. 15-19**, the P-values of peaks and the P-values of
682 the TFs were both obtained by running a linear regression ("lm" function in R) on 9,151 cells
683 (for pan-pituitary results) and 1,623 cells (for stem cell specific results). In addition, for the TFs
684 statistical analysis, the TFs are presented only if their Bonferroni-corrected P-values < 0.05.
685 Detailed statistics (such as t values of linear regression) are provided in **Supplementary Table**
686 **8**.

687

688 **Data availability**

689 The datasets (snRNAseq, snATACseq, sn multiome) generated in the present study are deposited
690 in GEO (accession # GSE178454). The sn human pituitary multi-omics atlas can be browsed via
691 a web-based portal accessible at snpituitaryatlas.princeton.edu. All datasets will also be
692 deposited with the Human Cell Atlas.

693

694 **Code availability**

695 Any computational code used in the paper is available upon request.

696

697 **Acknowledgements**

This work was supported by funding from the National Institute of Health (NIH) Grant DK46943 (SCS), Medical Research Council (MRC) Grant MR/T012153/1 (CLA), and Canadian Institutes of Health Research Project Grants PJT-162343 and -169184 (DJB). TLW was funded by King's College London as part of the "Cell Therapies and Regenerative Medicine" Four-Year Welcome Trust PhD Training Programme. We acknowledge the New York Genome Center for sequencing. Human tissue was obtained from the NIH NeuroBioBank. This work was supported in part through the computational and data resources and staff expertise provided by Scientific Computing at the Icahn School of Medicine at Mount Sinai.

Author contributions

ZZ, MZ, GRS, VY, and OGT contributed analytic tools and analyzed data; TLW contributed analytic tools, analyzed data, and performed research; NM, VDN, NS, MAA, and MV performed research; HP drafted the manuscript; SCS designed the study, analyzed, interpreted data, and drafted the manuscript, CLA, JLT and DJB analyzed, interpreted data, and drafted the manuscript; FRZ designed the study, performed research, analyzed and interpreted data, drafted the manuscript. All authors edited the manuscript and approved its final version.

Competing interests

The authors declare no competing interests.

Figure legends:

Figure 1: Experimental design for human pituitary cell type identification

721 **a**. Schematic of the overall experimental workflow, from procurement of the frozen pituitaries to
722 sn data analysis. **b**. Schematic summarizing sn data integration. For each sample, the
723 snATACseq dataset (colored dots UMAP) was integrated with the snRNAseq dataset (black
724 contours UMAP) to generate an integrated multi-omics overlay UMAP identifying cell types. On
725 the UMAP, cell types are color-coded and designated with a 2- to 3-letter code, as indicated on
726 the bottom key. The female pediatric pituitary sample is represented as an example. All
727 integrated samples are presented in **Supplementary Figs. 1** and **2**. **c.** Schematic of the
728 comparison between sn paired assays (same-sample sn multi-omics) (*i*) and sn mutiome assay
729 (same-cell) (*ii*). **d.** Same-cell sn multiome UMAP from the female pediatric sample (see
730 **Supplementary Table 1**).
731
732 **Figure 2: Merged analysis of same-sex human pituitary**
733 **a-d**. t-SNE representation of sn transcript expression (**a**, males; **c**, females) and of sn chromatin
734 accessibility (**b**, males; **d**, females) in the merged same-sex samples, with labeling by age of the
735 subject in each sex. Individual subjects are color-coded as indicated. Each cluster is identified by
736 a letter code as defined in **Fig.1**. Donor-related information is provided in **Supplementary Table**
737 **1**. **e**. Correlation between the cell type proportions identified by snRNAseq vs. snATACseq for
738 all samples (males and females). The linear regression is plotted. Pituitary cell types are color-
739 coded and the key is provided on the right.
740
741 **Figure 3: Identification of human stem cell sub-clusters by snRNAseq**
742 **a**. UMAP showing the stem cell cluster identification based on the snRNAseq data from the six
743 merged human pituitary samples. Each cell cluster is color-coded and numbered. Lineage-

committed progenitor stem cells are circled. **b**. UMAPs identifying all color-coded stem cell sub-clusters in females and males. The feature plot on the right shows *XIST* expression, highlighting the female samples. **c**. UMAPs identifying all color-coded stem cell sub-clusters in the pediatric, adult, and aged subjects. **d.** Feature plots depicting the expression distribution of key stem cell marker genes and of cell lineage commitment marker genes among the various clusters. A scale is included for each feature plot. All scales are similar except for *POMC* due to background gene expression. Additional gene feature plots are presented in **Supplementary Fig. 8**. **e**. Colocalization of *Sox2* (red) and *Jun* (blue) transcripts in a wild-type P56 CD-1 male adult mouse pituitary. Scale bar is 200µm. AL: anterior lobe; IL: intermediate lobe; PP: posterior pituitary. *Left*, full image. *Right*, magnification of the boxed region in the left panel. Arrows highlight specific cells with colocalization of *Sox2* and *Jun*. Refer to **Supplementary Fig. 10** for *Sox2* and *Jun* colocalization at P3 and P15. **f**. Gene expression analysis (violin plots at the right of each figure) and chromatin accessibility tracks analysis for *SOX2* (*Left*) and *GATA3* (*Right*) in all pituitary cell types from the sn multiome dataset generated from the pediatric female. The gene structure is presented below the tracks.

Figure 4: Characterization of coordinated gene expression and chromatin accessibility programs in human pituitary cell types

a, b. Heatmap of the levels of gene expression for the top human PSC LV ($LVsc_{rna}$) for each cell type and donor, top 30 genes are shown in (**a**) and top 200 genes in (**b**). Each pituitary sample is indicated at the top. In the scale bars, red signifies the highest level of RNA expression or chromatin accessibility. Pd, pediatric; Ad, adult; Ag, aged pituitary. **c.** Heatmap showing the top 200 genes associated with the human $LVsc_{rna}$ applied to the murine snRNAseq dataset[13]. **d.**

Heatmap showing the top 200 genes associated with the human $LVsc_{rna}$ applied to the human snATACseq datasets. (**a**, **b**, **c**, **d)** Cell type and subject color-coding are provided on the bottom key. Refer to **Supplementary Table 1** for donor-related information. Additional LV analyses are presented in **Supplementary Figs. 11 and 12**.

Figure 5: Age-associated chromatin accessibility and transcriptome pseudotime trajectory analysis

a. Heatmap showing the chromatin accessibility levels of the top 30 genes in the human age-dependent LV ($LVage_{atac}$). Cell type and subject color-coding are provided on the bottom of **Fig. 4**. Refer to **Supplementary Table 1** for donor-related information. Additional LV analyses are presented in **Supplementary Figs. 11** and **12**. **b.** Plot showing the overall changes in chromatin accessibility for all pituitary cell types over age for the females (*Left*) and the males (*Right*). Pituitary cell types are color-coded. The same cell types are linked with lines over age of the subjects. **c**. UMAP showing the trajectory within the stem cell cluster with samples color-coded by age for female (*Top*) and male (*Bottom*) samples. **d.** Pseudotime trajectory analysis for the female (*Top*) and male (*Bottom*) samples. The trajectories from each starting point head to the older samples. The color scale is shown for the pseudotime trajectories. **e.** Gene modules identified with pseudotime and showing changes over age. Monocle 3 identified groups of genes that change over as a function of pseudotime per sex. Trajectory variable genes were grouped into modules which were then plotted on a heatmap to show the relative expression of each gene module, within a sex, in each age group. The top 4 enriched modules for each age group are labelled, with module 1 being the most highly enriched in each age. Pd1-4 indicates the Pediatric top 4 modules, Ad1-4 represents the Adult enriched modules, and Ag1-4 marks the Aged

790 samples top 4 modules. Blue-red on the color scale represents low-high relative expression levels
791 (z-transformed mean expression) of gene modules. See **Supplementary Fig. 13** for selected
792 gene trajectories within specific modules. See **Supplementary Table 6** for the top genes per
793 modules.
794
795 **Figure 6: Linear model predicting the chromatin accessibility mechanisms and TFs**
796 **contributing to PSC gene expression**
797 **a**. Linear modeling analysis of all pituitary cells ("pan pituitary cell") infers the chromatin
798 accessibility and the TFs involved in stem cell-specific *SOX2* expression (*Left*, top track is the
799 contribution of each peak to gene expression measured by -log(P-value), and bottom tracks are
800 the TFs binding sites). The individual contribution of each predicted TF to *SOX2* expression is
801 shown as -log(P-values, *Right*). See **Supplementary Fig. 18** for *SOX2* analysis in stem cells
802 only. **b**. Pan pituitary cell analysis infers the chromatin accessibility and the TFs involved in
803 stem cell-specific *GATA3* expression (*Top*, top track is the contribution of each peak to gene
804 expression measured by -log(P-value), and bottom tracks are the TFs binding sites). The
805 individual contribution of each predicted TF to *GATA3* expression is shown as -log(P-values)
806 (*Right*). **c**. Linear modeling analysis in stem cells only infers the chromatin accessibility and the
807 TFs involved in the differential expression of *GATA3* expression within the stem cell population.
808 No TFs are predicted to contribute to *GATA3* expression in stem cells. **d**. Linear modeling
809 analysis in stem cells only infers the chromatin accessibility and the TFs involved in the
810 differential expression of *POMC* expression (*Left*, top track is the contribution of each peak to
811 gene expression measured by -log(P-value), and bottom tracks are the TFs binding sites). The

812 individual contribution of each predicted TF to *POMC* expression is shown as log(P-values)
813 (*Right*). See **Supplementary Fig. 17** for pan pituitary cell analysis of *POMC* expression.
814
815 **REFERENCES:**
816

817 1. Morris SA. The evolving concept of cell identity in the single cell era. *Development* **146**,
818 (2019).
819
820 2. Tanay A, Regev A. Scaling single-cell genomics from phenomenology to mechanism.
821 *Nature* **541**, 331-338 (2017).
822
823 3. Griffiths JA, Scialdone A, Marioni JC. Using single-cell genomics to understand
824 developmental processes and cell fate decisions. *Mol Syst Biol* **14**, e8046 (2018).
825
826 4. Han X, *et al.* Construction of a human cell landscape at single-cell level. *Nature* **581**,
827 303-309 (2020).
828
829 5. Zhang S, *et al.* Single-cell transcriptomics identifies divergent developmental lineage
830 trajectories during human pituitary development. *Nat Commun* **11**, 5275 (2020).
831
832 6. Project E. ENCODE: Encyclopedia of DNA Elements.) (2021).
833
834 7. Consortium EP, *et al.* Expanded encyclopaedias of DNA elements in the human and
835 mouse genomes. *Nature* **583**, 699-710 (2020).
836
837 8. Castinetti F, Davis SW, Brue T, Camper SA. Pituitary stem cell update and potential
838 implications for treating hypopituitarism. *Endocr Rev* **32**, 453-471 (2011).
839
840 9. Andoniadou CL, *et al.* Sox2(+) stem/progenitor cells in the adult mouse pituitary support
841 organ homeostasis and have tumor-inducing potential. *Cell Stem Cell* **13**, 433-445 (2013).
842
843 10. Rizzoti K, Akiyama H, Lovell-Badge R. Mobilized adult pituitary stem cells contribute to
844 endocrine regeneration in response to physiological demand. *Cell Stem Cell* **13**, 419-432
845 (2013).
846
847 11. Vankelecom H. Pituitary Stem Cells: Quest for Hidden Functions. In: *Stem Cells in*
848 *Neuroendocrinology* (eds Pfaff D, Christen Y) (2016).
849
850 12. Russell JP, Lodge EJ, Andoniadou CL. Basic Research Advances on Pituitary Stem Cell
851 Function and Regulation. *Neuroendocrinology* **107**, 196-203 (2018).
852

13. Ruf-Zamojski F, *et al.* Single nucleus multi-omics regulatory landscape of the murine pituitary. *Nat Commun* **12**, 2677 (2021).

14. Cheung LYM, *et al.* Single-Cell RNA Sequencing Reveals Novel Markers of Male Pituitary Stem Cells and Hormone-Producing Cell Types. *Endocrinology* **159**, 3910-3924 (2018).

15. Russell JP, *et al.* Pituitary stem cells produce paracrine WNT signals to control the expansion of their descendant progenitor cells. *Elife* **10**, (2021).

16. Ben-Shlomo A, Liu NA, Melmed S. Somatostatin and dopamine receptor regulation of pituitary somatotroph adenomas. *Pituitary* **20**, 93-99 (2017).

17. Lodge EJ, *et al.* Homeostatic and tumourigenic activity of SOX2+ pituitary stem cells is controlled by the LATS/YAP/TAZ cascade. *Elife* **8**, (2019).

18. Cox B, Roose H, Vennekens A, Vankelecom H. Pituitary stem cell regulation: who is pulling the strings? *J Endocrinol* **234**, R135-R158 (2017).

19. Loda A, Heard E. Xist RNA in action: Past, present, and future. *PLoS Genet* **15**, e1008333 (2019).

20. Semba T, Sammons R, Wang X, Xie X, Dalby KN, Ueno NT. JNK Signaling in Stem Cell Self-Renewal and Differentiation. *Int J Mol Sci* **21**, (2020).

21. Pagin M, *et al.* Sox2 controls neural stem cell self-renewal through a Fos-centered gene regulatory network. *Stem Cells*, (2021).

22. Budry L, *et al.* The selector gene Pax7 dictates alternate pituitary cell fates through its pioneer action on chromatin remodeling. *Genes Dev* **26**, 2299-2310 (2012).

23. Schluter H, Stark HJ, Sinha D, Boukamp P, Kaur P. WIF1 is expressed by stem cells of the human interfollicular epidermis and acts to suppress keratinocyte proliferation. *J Invest Dermatol* **133**, 1669-1673 (2013).

24. Poggi L, Casarosa S, Carl M. An Eye on the Wnt Inhibitory Factor Wif1. *Front Cell Dev Biol* **6**, 167 (2018).

25. Karlsson G, *et al.* Smad4 is critical for self-renewal of hematopoietic stem cells. *J Exp Med* **204**, 467-474 (2007).

26. Avery S, Zafarana G, Gokhale PJ, Andrews PW. The role of SMAD4 in human embryonic stem cell self-renewal and stem cell fate. *Stem Cells* **28**, 863-873 (2010).

27. Kandyba E, Hazen VM, Kobielak A, Butler SJ, Kobielak K. Smad1 and 5 but not Smad8 establish stem cell quiescence which is critical to transform the premature hair follicle during morphogenesis toward the postnatal state. *Stem Cells* **32**, 534-547 (2014).

28. Haston S, Manshaei S, Martinez-Barbera JP. Stem/progenitor cells in pituitary organ homeostasis and tumourigenesis. *J Endocrinol* **236**, R1-R13 (2018).

29. Mao W, Zaslavsky E, Hartmann BM, Sealfon SC, Chikina M. Pathway-level information extractor (PLIER) for gene expression data. *Nat Methods* **16**, 607-610 (2019).

30. Trapnell C, *et al.* The dynamics and regulators of cell fate decisions are revealed by pseudotemporal ordering of single cells. *Nat Biotechnol* **32**, 381-386 (2014).

31. Cao J, *et al.* Joint profiling of chromatin accessibility and gene expression in thousands of single cells. *Science* **361**, 1380-1385 (2018).

32. Ma S, *et al.* Chromatin Potential Identified by Shared Single-Cell Profiling of RNA and Chromatin. *Cell* **183**, 1103-1116 e1120 (2020).

33. Pulichino AM, Vallette-Kasic S, Tsai JP, Couture C, Gauthier Y, Drouin J. Tpit determines alternate fates during pituitary cell differentiation. *Genes Dev* **17**, 738-747 (2003).

34. Brinkmeier ML, *et al.* TCF and Groucho-related genes influence pituitary growth and development. *Mol Endocrinol* **17**, 2152-2161 (2003).

35. Kioussi C, *et al.* Identification of a Wnt/Dvl/beta-Catenin --> Pitx2 pathway mediating cell-type-specific proliferation during development. *Cell* **111**, 673-685 (2002).

36. Pacini V, Petit F, Querat B, Laverriere JN, Cohen-Tannoudji J, L'Hote D. Identification of a pituitary ERalpha-activated enhancer triggering the expression of Nr5a1, the earliest gonadotrope lineage-specific transcription factor. *Epigenetics Chromatin* **12**, 48 (2019).

37. Vult von Steyern F, Martinov V, Rabben I, Nja A, de Lapeyriere O, Lomo T. The homeodomain transcription factors Islet 1 and HB9 are expressed in adult alpha and gamma motoneurons identified by selective retrograde tracing. *Eur J Neurosci* **11**, 2093-2102 (1999).

38. Harrison KA, Druey KM, Deguchi Y, Tuscano JM, Kehrl JH. A novel human homeobox gene distantly related to proboscipedia is expressed in lymphoid and pancreatic tissues. *J Biol Chem* **269**, 19968-19975 (1994).

39. Li H, Arber S, Jessell TM, Edlund H. Selective agenesis of the dorsal pancreas in mice lacking homeobox gene Hlxb9. *Nat Genet* **23**, 67-70 (1999).

40. Hsu J, *et al.* E2F4 regulates transcriptional activation in mouse embryonic stem cells independently of the RB family. *Nat Commun* **10**, 2939 (2019).

41. Budry L, *et al.* Related pituitary cell lineages develop into interdigitated 3D cell networks. *Proc Natl Acad Sci U S A* **108**, 12515-12520 (2011).

42. Li S, Crenshaw EB, 3rd, Rawson EJ, Simmons DM, Swanson LW, Rosenfeld MG. Dwarf locus mutants lacking three pituitary cell types result from mutations in the POU-domain gene pit-1. *Nature* **347**, 528-533 (1990).

43. Charles MA, *et al.* Pituitary-specific Gata2 knockout: effects on gonadotrope and thyrotrope function. *Mol Endocrinol* **20**, 1366-1377 (2006).

44. Mathys H, *et al.* Single-cell transcriptomic analysis of Alzheimer's disease. *Nature* **570**, 332-337 (2019).

45. Butler A, Hoffman P, Smibert P, Papalexi E, Satija R. Integrating single-cell transcriptomic data across different conditions, technologies, and species. *Nat Biotechnol* **36**, 411-420 (2018).

46. Stuart T, *et al.* Comprehensive Integration of Single-Cell Data. *Cell* **177**, 1888-1902 e1821 (2019).

47. Stuart T, Srivastava A, Lareau C, Satija R. Multimodal single-cell chromatin analysis with Signac. *bioRxiv*, 2020.2011.2009.373613 (2020).

48. Hafemeister C, Satija R. Normalization and variance stabilization of single-cell RNA-seq data using regularized negative binomial regression. *Genome Biol* **20**, 296 (2019).

49. Hao Y, *et al.* Integrated analysis of multimodal single-cell data. *bioRxiv*, 2020.2010.2012.335331 (2020).

50. Cao J, *et al.* The single-cell transcriptional landscape of mammalian organogenesis. *Nature* **566**, 496-502 (2019).

51. Pliner HA, *et al.* Cicero Predicts cis-Regulatory DNA Interactions from Single-Cell Chromatin Accessibility Data. *Mol Cell* **71**, 858-871 e858 (2018).

a

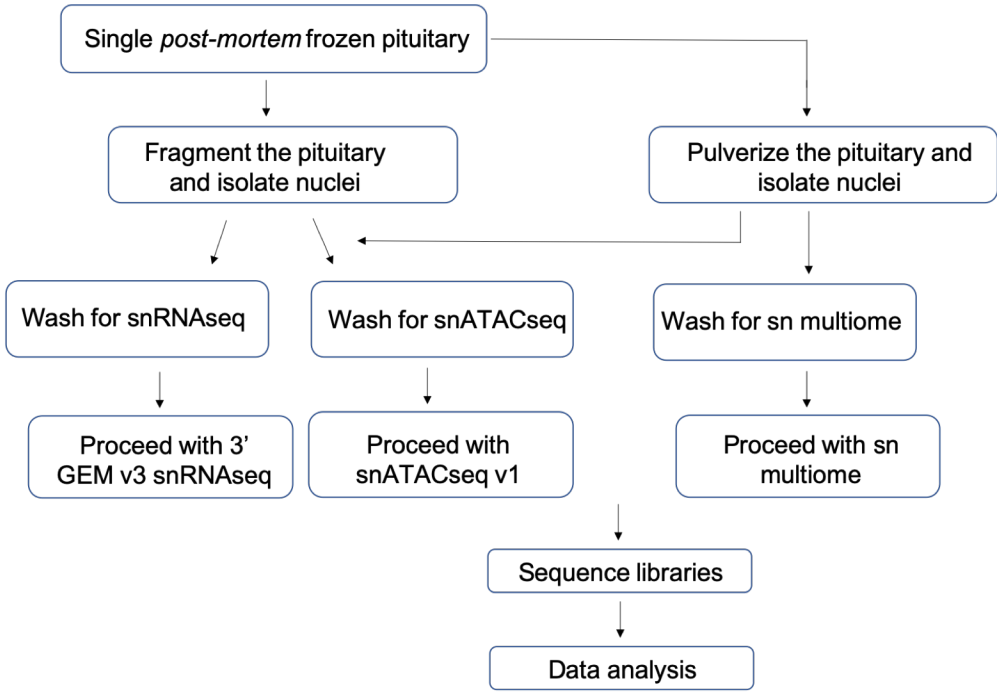

b.

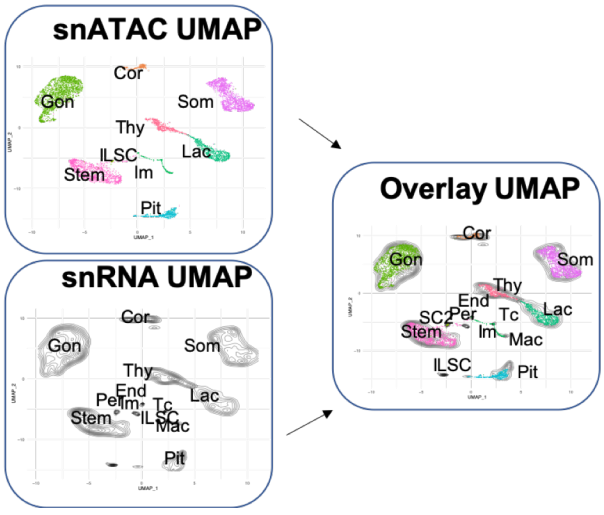

c. *i.* sn paired assays *ii.* sn multiome assay

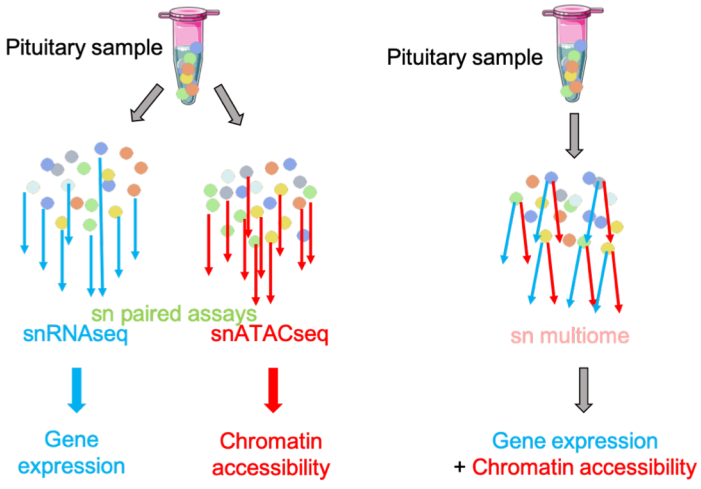

- Corticotropes (Cor)
- Endothelial cells (End)
- Intermediate lobe stem cells (ILSC)
- Gonadotropes (Gon)
- Immune cells (Im)
- Lactotropes (Lac)
- Macrophages (Mac)
- Pericytes (Per)
- Pituicytes (Pit)
- Stem cells 2 (SC2)
- Somatotropes (Som)
- Stem cells (Stem)
- T cells (TC)
- Thyrotropes (Thy)

d.

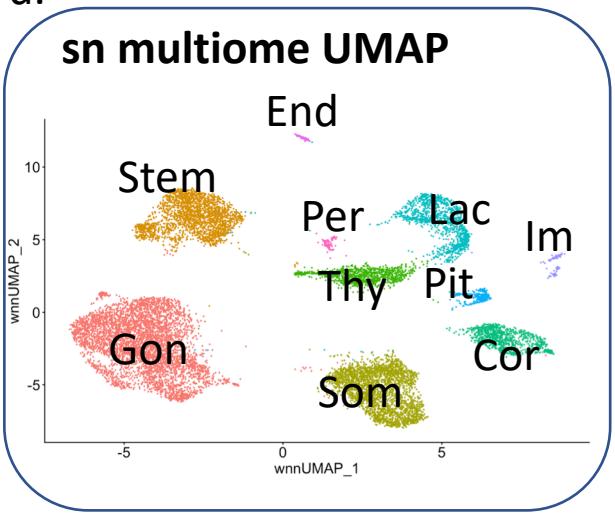

Figure 1

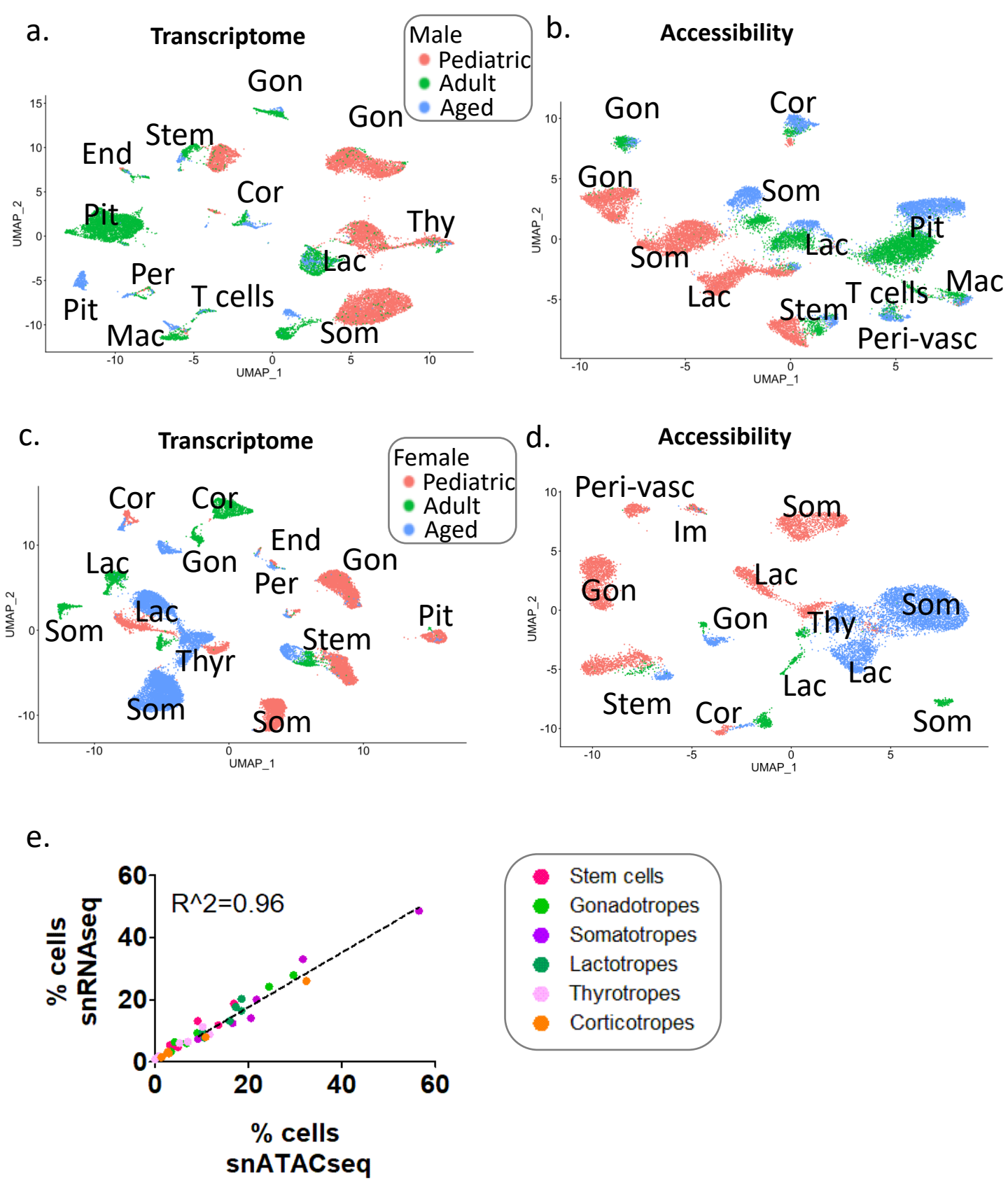
a.
Transcriptome
Male
Pediatric
Adult
Aged
Gon
Gon
Stem
End
Cor
Pit
Thy
Lac
Per
T cells
Pit
Mac
Som
UMAP_1
UMAP_2
b.
Accessibility
Gon
Cor
Gon
Som
Pit
Lac
Som
Lac
T cells
Mac
Stem
Peri-vasc
c.
Transcriptome
Female
Pediatric
Adult
Aged
Cor
Cor
End
Lac
Gon
Gon
Per
Lac
Pit
Som
Stem
Thyr
Som
Som
d.
Accessibility
Peri-vasc
Som
Im
Lac
Gon
Som
Gon
Thy
Lac
Lac
Stem
Cor
Som
e.
R^2=0.96
% cells snRNAseq
% cells snATACseq
Stem cells
Gonadotropes
Somatotropes
Lactotropes
Thyrotropes
Corticotropes

Figure 2

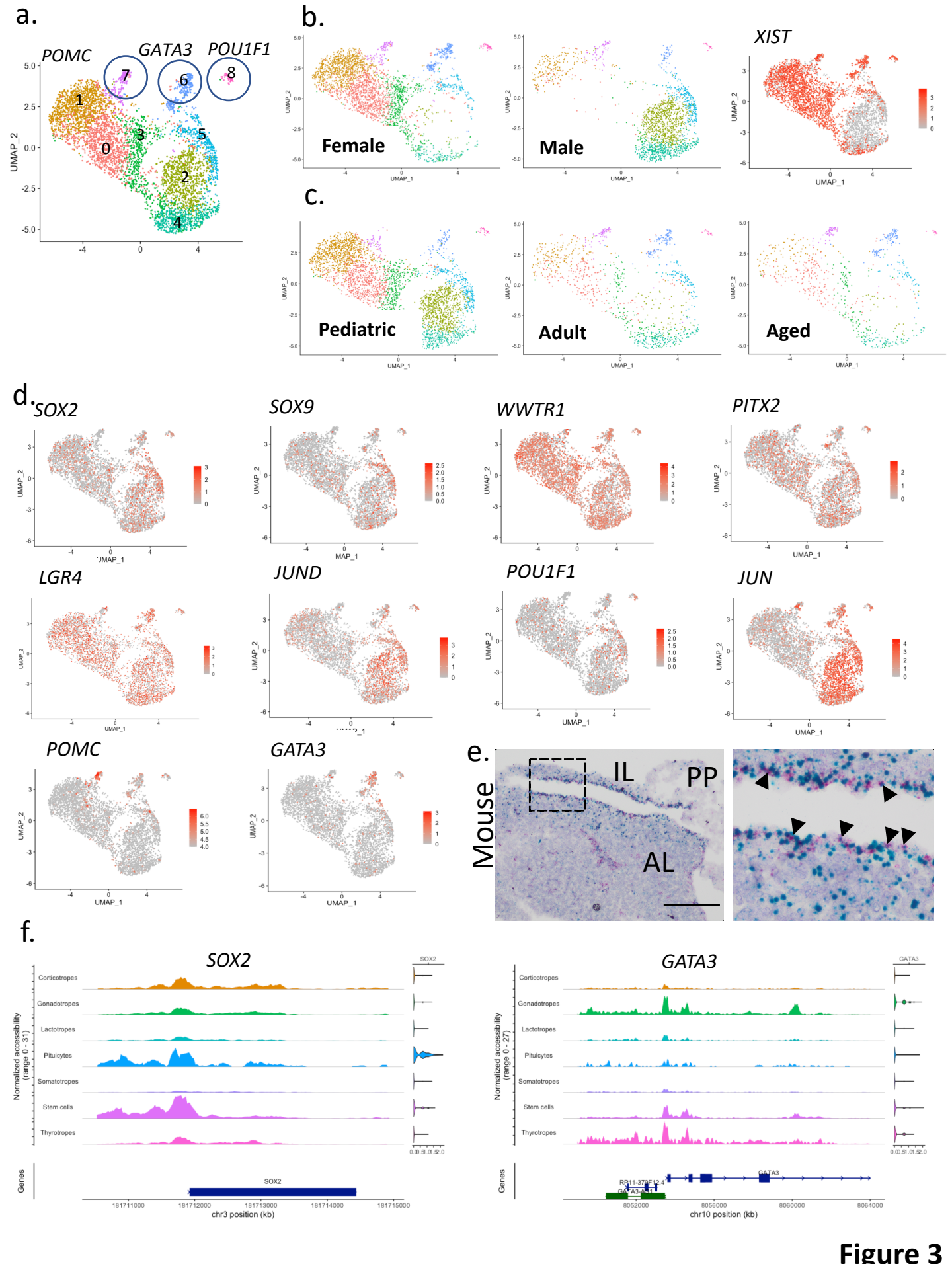
a.
POMC
GATA3
POU1F1
b.
Female
Male
XIST
c.
Pediatric
Adult
Aged
d.
SOX2
SOX9
WWTR1
PITX2
LGR4
JUND
POU1F1
JUN
POMC
GATA3
e.
Mouse
IL
PP
AL
f.
SOX2
GATA3
Corticotropes
Gonadotropes
Lactotropes
Pituicytes
Somatotropes
Stem cells
Thyrotropes
Normalized accessibility
Genes
chr3 position (kb)
chr10 position (kb)

Figure 3

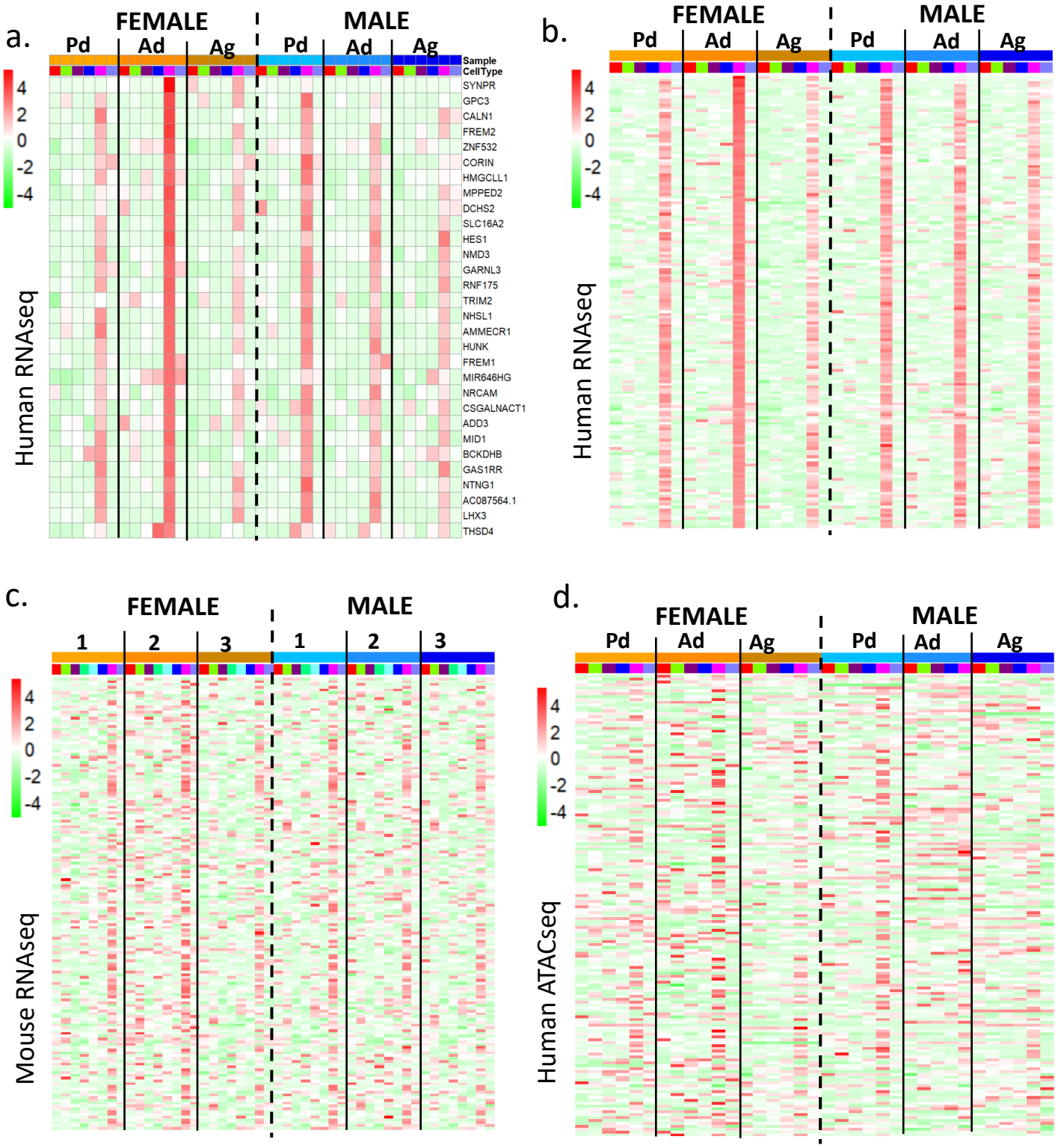

Cell type

- Corticotrope
- Gonadotrope
- Lactotrope
- Somatotrope
- Stem cell
- Thyrotrope

sample

- Pediatric (Pd) female or Female mouse 1
- Adult (Ad) female or Female mouse 2
- Aged (Ag) female or Female mouse 3
- Pediatric (Pd) male or Male mouse 1
- Adult (Ad) male or Male mouse 2
- Aged (Ag) male or Male mouse 3

Figure 4

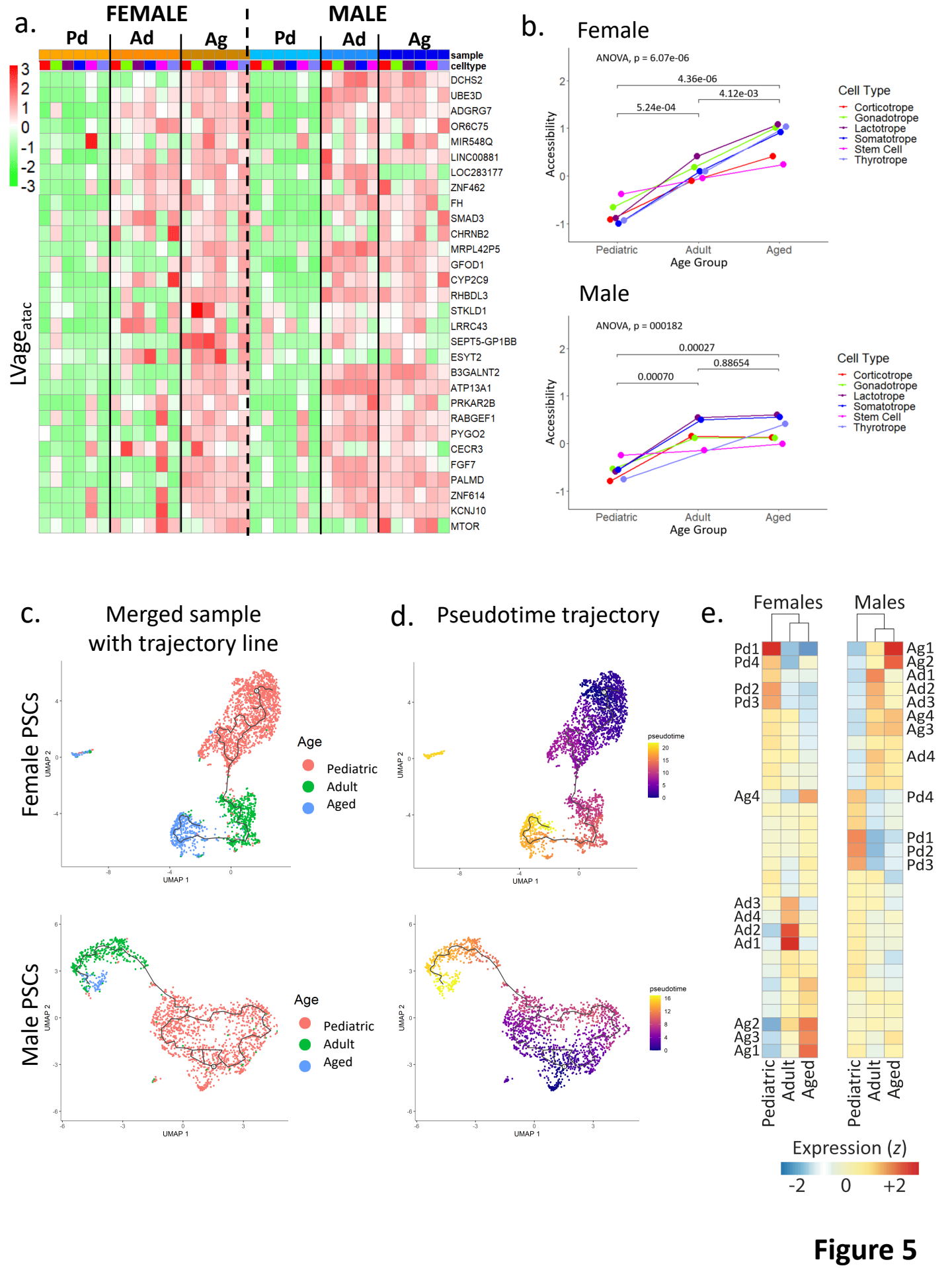
a.
FEMALE
MALE
Pd
Ad
Ag
Pd
Ad
Ag
sample
celltype
3
2
1
0
-1
-2
-3
LVage atac
DCHS2
UBE3D
ADGRG7
OR6C75
MIR548Q
LINC00881
LOC283177
ZNF462
FH
SMAD3
CHRNB2
MRPL42P5
GFOD1
CYP2C9
RHBDL3
STKLD1
LRRC43
SEPT5-GP1BB
ESYT2
B3GALNT2
ATP13A1
PRKAR2B
RABGEF1
PYGO2
CECR3
FGF7
PALMD
ZNF614
KCNJ10
MTOR
b.
Female
ANOVA, p = 6.07e-06
4.36e-06
4.12e-03
5.24e-04
Accessibility
Pediatric
Adult
Aged
Age Group
Cell Type
Corticotrope
Gonadotrope
Lactotrope
Somatotrope
Stem Cell
Thyrotrope
Male
ANOVA, p = 000182
0.00027
0.88654
0.00070
Accessibility
Pediatric
Adult
Aged
Age Group
Cell Type
Corticotrope
Gonadotrope
Lactotrope
Somatotrope
Stem Cell
Thyrotrope
c.
Merged sample
with trajectory line
Female PSCs
Male PSCs
UMAP 1
UMAP 2
Age
Pediatric
Adult
Aged
d.
Pseudotime trajectory
pseudotime
UMAP 1
UMAP 2
e.
Females
Males
Pd1
Pd4
Pd2
Pd3
Ag4
Ad3
Ad4
Ad2
Ad1
Ag2
Ag3
Ag1
Ag1
Ag2
Ad1
Ad2
Ad3
Ag4
Ag3
Ad4
Pd4
Pd1
Pd2
Pd3
Pediatric
Adult
Aged
Expression (z)
-2
0
+2

Figure 5

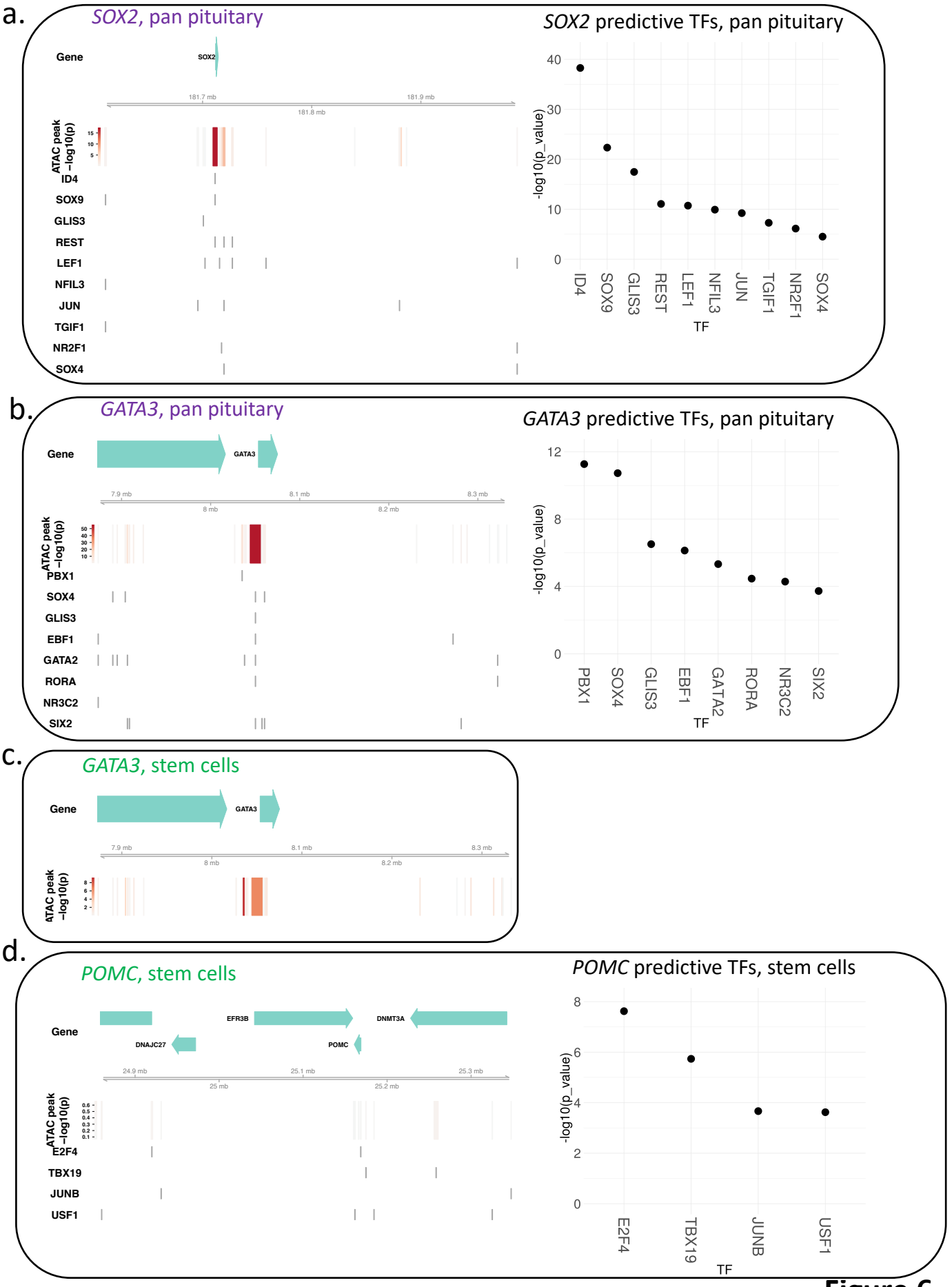
a.
SOX2, pan pituitary
Gene
SOX2
181.7 mb
181.8 mb
181.9 mb
ATAC peak −log10(p)
ID4
SOX9
GLIS3
REST
LEF1
NFIL3
JUN
TGIF1
NR2F1
SOX4
SOX2 predictive TFs, pan pituitary
-log10(p_value)
40
30
20
10
0
ID4
SOX9
GLIS3
REST
LEF1
NFIL3
JUN
TGIF1
NR2F1
SOX4
TF
b.
GATA3, pan pituitary
Gene
GATA3
7.9 mb
8 mb
8.1 mb
8.2 mb
8.3 mb
ATAC peak −log10(p)
PBX1
SOX4
GLIS3
EBF1
GATA2
RORA
NR3C2
SIX2
GATA3 predictive TFs, pan pituitary
-log10(p_value)
12
8
4
0
PBX1
SOX4
GLIS3
EBF1
GATA2
RORA
NR3C2
SIX2
TF
c.
GATA3, stem cells
Gene
GATA3
7.9 mb
8 mb
8.1 mb
8.2 mb
8.3 mb
ATAC peak −log10(p)
d.
POMC, stem cells
Gene
EFR3B
DNMT3A
DNAJC27
POMC
24.9 mb
25 mb
25.1 mb
25.2 mb
25.3 mb
ATAC peak −log10(p)
E2F4
TBX19
JUNB
USF1
POMC predictive TFs, stem cells
-log10(p_value)
8
6
4
2
0
E2F4
TBX19
JUNB
USF1
TF

Figure 6